

Simple dense-pattern optical multipass cells

Joel A. Silver

Multiple-pass optical cells with dense spot patterns are useful for many applications, especially when the cell volume must be minimized relative to the optical path length. Present methods to achieve these dense patterns require expensive, highly precise astigmatic mirrors and complex alignment procedures. This work describes a new, simpler, and less demanding mirror system, comprising either a pair of cylindrical mirrors or one cylindrical and one spherical mirror. © 2005 Optical Society of America

OCIS codes: 300.1030, 300.6380, 220.4830.

1. Introduction

Multiple pass optical cells are used to achieve very long optical path lengths in a small volume and have been extensively used for absorption spectroscopy,^{1,2} laser delay lines,³ Raman gain cells,⁴ interferometers,⁵ photoacoustic spectroscopy,⁶ and other resonators.^{7,8} These cells have taken the form of White cells¹ and their variants,⁹ integrating spheres,¹⁰ and stable resonator cavities.⁷

The stable resonator is typified by the design of Herriott *et al.*⁵ The simplest such cell consists of two spherical mirrors of equal focal lengths separated by a distance d less than or equal to four times the focal lengths f of the mirrors. A laser beam is injected through a hole in one of the mirrors; the hole is typically located near the mirror edge. The beam is periodically reflected and refocused between the mirrors and then, after a designated number of passes N , exits through the input hole (corresponding exactly to the entry position of the input beam, defining the reentrant condition) in a direction (slope) that is different from the entry slope. As a result, the total optical path traversed in the cell is approximately $N \times d$. The pattern of reflected spots observed on the mirrors in these cells forms an ellipse. Excellent descriptions for the design, setup, and use of these cells are given by Altmann *et al.*² and McManus and Keabian.¹¹

When the cell volume must be minimized relative to the optical path length or when a very long optical path (>50 m) or very small footprint is desired, it is useful to increase the density of passes per unit volume of cell. The conventional spherical mirror Herriott cell is limited by the number of spots one can fit along the path of the ellipse without the spot adjacent to the output hole being clipped by or exiting that hole at a pass number less than N . This restricts the total number of passes to approximately the circumference of the ellipse divided by the hole diameter, which in turn is limited by the laser beam diameter. For a 25 mm radius mirror with a relatively small 3 mm diameter input hole located 20 mm from the center of the mirror, a maximum of about $(2\pi \times 20)/3 \approx 40$ spots, or 80 passes, is possible at best. Generally the hole is made larger to prevent any clipping of the laser input beam that might lead to undesirable interference fringes, and typical spherical Herriott cells employ less than 60 passes.

Herriott and Schulte³ demonstrated that the use of a pair of astigmatic mirrors could greatly increase the spot density and hence optical path length, in the cell. Each mirror has slightly different focal lengths (f_x and f_y) along orthogonal x and y axes, and the mirrors are aligned with the same focal lengths parallel to one another. The resulting spots of each reflection on the mirrors create precessions of ellipses to form Lissajous patterns. Since these patterns are distributed about the entire face of each mirror, many more spots can be accommodated than in a cell with spherical mirrors. McManus *et al.*¹² outlined the theory and behavior of this astigmatic Herriott cell and showed that the density of passes can be increased by factors of three or more over spherical mirror cells. For these astigmatic mirror cells, light is injected through a hole in the center of the input mirror. Allowed solutions for reentrant configurations are

J. Silver (jsilver@SWSciences.com) is with Southwest Sciences, Inc., 1570 Pacheco Street, Suite E-11, Santa Fe, New Mexico 87505-3993.

Received 3 January 2005; revised manuscript received 29 March 2005; accepted 30 March 2005.

0003-6935/05/316545-12\$15.00/0

© 2005 Optical Society of America

characterized by a pair of integer indices M_x and M_y , since there are now two focal lengths present along orthogonal axes.

The drawback of this design is that the constraints to achieve useful operation are rather severe. First of all, both M_x and M_y must simultaneously be reentrant, so that for a desired N and variable distance d , the focal lengths f_x and f_y must be specified to a tolerance of one part in 10^4 . Since mirrors can rarely be manufactured to such tolerances, this cell as originally proposed is impractical. However, Keabian¹³ devised a method to make the astigmatic cell usable. Starting with the astigmatic Herriott setup with mirror axes aligned, he rotates one mirror relative to the other around the z axis, thereby mixing the (previously independent) x and y components of the beam coordinates. A moderate rotation of ~ 5 – 20 deg and a small compensating adjustment of the mirror separation distance can accommodate the imprecision in the manufacturing of the mirror focal lengths. However, this approach is still difficult to achieve in practice and requires complex calculations and skill to get to the desired pattern. Furthermore, the astigmatic mirrors must be custom made and cost many thousands of dollars for a single pair.

Recently, Hao *et al.*¹⁴ described another way to generate dense Lissajous patterns by using a pair of cylindrical mirrors, each having a different focal length, where the principal axes of the mirrors are always orthogonal to one another. In essence, this creates a pair of mirrors whose x -axis component comprises one curved surface (on mirror A) of focal length f_x and one flat mirror surface (on mirror B), and along the y axis one flat mirror surface (on mirror A) and one curved surface of focal length f_y (on mirror B), where $f_x \neq f_y$. Formulas to predict the spot patterns on each mirror are provided. The advantage of this system is that dense Lissajous patterns can be formed from a pair of inexpensive mirrors, in contrast to the requirement for custom astigmatic mirrors. The drawback of this mismatched focal length pair of cylindrical mirrors is that there are few reentrant solutions permitted. Of course, for photoacoustic measurements as intended by Hao, where any exiting light is not detected, the light does not necessarily have to be reentrant, and many values of mirror separation that are not reentrant, but do generate many passes, are useful.

In this work we present a much simpler and more flexible approach for achieving dense multipass cells by using inexpensive cylindrical mirrors.¹⁵ In one case two cylindrical mirrors can be used to create a wide diversity of reentrant patterns as well as to generate conventional elliptical patterns. Alternatively, one can also utilize a cylindrical–spherical mirror pair with near reentrant solutions. This latter approach has not been considered a viable method in the past, but exact reentry is not a necessary criterion for practical use and simplifies use in many cases. With the spherical–cylindrical mirror pair, there are very few or no exact reentrant solutions (depending

on the focal lengths of the mirrors). But a limited number of useful nearly reentrant solutions exist. Unlike all other dense cell methods, neither of these cells is sensitive to the tolerances of the manufactured focal lengths but are sensitive only to the relative mirror separation ratio d/f .

2. Theory

A. Conventional Herriott Cells

As generally configured, the normal Herriott cell comprises one spherical mirror (“front”) of focal length f with an off-axis entrance hole at coordinates $[x_0, y_0]$, through which a laser beam is injected with slopes x_0' and y_0' and pointed at a second spherical mirror (“rear”), also of focal length f . This beam is then periodically reflected and refocused such that the beam eventually exits through the center of the input hole at $[x_0, y_0]$, defining the reentrant condition, but in the opposite direction (slope) of the input beam so as to make possible the placement of a detector without obstructing the input beam. The conditions for reentry and the number of passes in the cell (even integer N) are governed by the focal lengths of the mirrors f , their separation d , and the initial slope of the input beam. For brevity, the formulas and detailed descriptions are not presented here but can be found in Refs. 2 and 11. The patterns of spots on the mirrors trace out an ellipse, where each spot location is characterized by multiples i of an advance angle θ . For the off-axis injection of the laser beam, light exits the cell exactly at $[x_0, y_0]$ only when an integral multiple of θ equals 2π , so that

$$\theta_R = 2\pi M/N, \quad d = 2f(1 - \cos \theta_R), \quad (1)$$

where the number of complete orbits of spots before the beam exits is denoted by the integer index M ; θ_R is the angular projection advance angle for each sequential pass for this reentry condition. Thus after N passes the spot pattern has rotated a multiple of 2π in both x and y coordinates, and the beam exits through the input hole. While many possible solutions for N and M exist for any given set of input conditions, the generally used initial condition (with the off-axis input hole location defined as $[x_0 = 0, y_0 = 1]$ and the mirror separation d set equal to $2f$) is to align the first pass at $x_1 = 1, y_1 = 0$ (i.e., input slopes corresponding to $x_0' = 1, y_0' = -1$). This condition generates a circle with $N = 4$ at $d = 2f$. Under these conditions, all patterns can be characterized by $N = 4M \pm K$, where K is an even integer and positive K corresponds to solutions of $d < 2f$ and negative K to solutions for $d > 2f$ (up to a maximum allowed separation of $4f$).

In general, $-K$ solutions are not as useful, since these spot patterns trend toward being much larger in radius relative to the input hole position as the mirror separation increases beyond $2f$, causing the pattern to walk off the edge of the mirror. While many different (M, N) pairs can generate the angular advance angle θ_R in Eqs. (1), only the set with the

lowest N is allowed. All other sets cannot be achieved, since the pattern will exit at a pass number less than N . As elaborated by McManus and Keabian,¹¹ these rules can be formalized by computing modulo orders of the corresponding K values for any N .

The useful properties of the spherical Herriott cell are that (1) virtually any desired optical path length and number of passes can be achieved by simply adjusting the mirror separation distance, (2) the output spot position and slope are fixed regardless of the spot pattern or number of passes, and (3) this output is invariant to slight tilt or misalignment of the mirrors. Thus once the initial beam is aligned and the detector located, the number of passes and path length are readily adjusted by simply moving the position of the rear mirror along the axis.

B. High-Density Cells

In order to achieve a higher density of spots, which leads to longer path lengths for the same sized cell, Herriott developed a multipass optical cell that uses a pair of matched astigmatic mirrors.³ Each mirror has a different finite focal length along its orthogonal x and y axes, f_x and f_y . Unlike the spherical cell, the astigmatic cell x and y coordinates have separate, independent solutions. With the input hole now in the center of the mirror, the x and y coordinates for the i th spot are defined by

$$\begin{aligned} x_i &= X_{\max} \sin(i\theta_x), \\ y_i &= Y_{\max} \sin(i\theta_y), \\ \theta_{xR} &= \cos^{-1}(1 - d/2f_x) = \pi M_x/N, \\ \theta_{yR} &= \cos^{-1}(1 - d/2f_y) = \pi M_y/N, \end{aligned} \quad (2)$$

where X_{\max} and Y_{\max} are the maximum positions of x and y in the spot pattern and the R subscript on advance angles θ denotes reentrant conditions.

The reentrant solutions shown here for M_x and M_y are slightly different than in Eqs. (1) because the beam can exit after only π rad for a central hole, rather than a full 2π when the input hole is at the edge of the mirror. Here M can be viewed as the number of half-orbits of spots before each coordinate exits. As a result, the allowed indices are now defined by $N = 2M_x + K_x = 2M_y + K_y$.

To achieve reentrant conditions, two simultaneous equations must be solved for a desired set of $\{N, M_x, M_y\}$. This results in specific design values for $d, f_x,$ and f_y , making the system much less flexible than the spherical Herriott cell for being able to select N , given a particular set of mirrors. Since both half-orbits and full orbits of the spot patterns can be reentrant for the astigmatic cell, the beam can exit into any quadrant of x - y space. Optimal solutions can be found where the beam exits in a plane opposite the input beam onto a unique, fixed position, where patterns minimize spots near the input hole, and where common factors (lower-order exits at passes $<N$) are

avoided. It has been determined that these solutions require that $N/2$ be an odd integer and M_x and M_y be even integers.¹²

To achieve a reentrant design, manufacturing criteria on the precision for $d, f_x,$ and f_y are so severe that a commercially produced cell is almost impossible to make reliably and repeatedly. The focal lengths must be precise to better than 1 part in 10^4 . Keabian¹³ devised a method to make the astigmatic cell usable by rotating the axis of one astigmatic mirror relative to the other and thereby mixing the (previously independent) x and y components of the beam coordinates. A moderate rotation of ~ 5 – 20 deg and a small compensating adjustment of the mirror separation distance can accommodate the imprecision in the manufacturing of the mirror focal lengths.

The cylindrical cell of Hao *et al.*¹⁴ uses two cylindrical mirrors of differing focal lengths with orthogonally opposed curvatures. This is essentially equivalent to folding the astigmatic cell by using a plane mirror (i.e., making an equivalent astigmatic cell that uses one plane and one astigmatic mirror) and then transferring one curved axis to the plane mirror. As a result, this design as originally conceived still has the problem with manufacturing tolerances.

C. Numerical Determination of Spot Patterns

In all of these Herriott-style systems, the precise patterns of spot locations can be computed either directly from matrix multiplication methods or from analytic solutions of the relevant ray-tracing equations derived from these matrices.

Ray matrix theory as outlined by Yariv⁷ describes the propagation of light rays through an optical system. Given the x_0 and y_0 coordinates and respective slopes x_0' and y_0' of the incident ray, the positions and slopes after each action (translation, reflection, etc.) can be found. These slopes and positions can be represented by a vector \mathbf{r} , where the $(i + 1)$ th pass is related to the previous pass i by a square matrix \mathbf{M} containing coefficients that perform the specified optical operation:

$$\mathbf{r}_{i+1} = \begin{bmatrix} x_{i+1} \\ x_{i+1}' \\ y_{i+1} \\ y_{i+1}' \end{bmatrix} = \mathbf{M} \cdot \mathbf{r}_i = [4 \times 4] \begin{bmatrix} x_i \\ x_i' \\ y_i \\ y_i' \end{bmatrix}. \quad (3)$$

For the case of two mirrors, we can find the position and slopes of the ray after one round trip of the cell, denoted by subscript n , as the product $\mathbf{R}_1 \cdot \mathbf{D} \cdot \mathbf{R}_2 \cdot \mathbf{D} \equiv \mathbf{C}$, where \mathbf{R} is a reflection matrix, \mathbf{D} a translation matrix, and the subscripts 1 and 2 correspond to the front and rear mirrors, respectively. The relevant matrices for translation and reflection, where f is the focal length along the specified component axis and d the separation, are

$$\mathbf{D} = \begin{bmatrix} 1 & d & 0 & 0 \\ 0 & 1 & 0 & 0 \\ 0 & 0 & 1 & d \\ 0 & 0 & 0 & 1 \end{bmatrix}, \quad \mathbf{R} = \begin{bmatrix} 1 & 0 & 0 & 0 \\ -1/f_x & 1 & 0 & 0 \\ 0 & 0 & 1 & 0 \\ 0 & 0 & -1/f_y & 1 \end{bmatrix}. \quad (4)$$

For n round trips, \mathbf{r}_n is then equal to $\mathbf{C}^n \cdot \mathbf{r}_0$.

If the x and y components are uncoupled, then we can separate 2×2 submatrices for the x and y components in Eq. (4), and the four elements of the solution \mathbf{C} for x or y can be expressed as

$$\mathbf{C} = \begin{bmatrix} A & B \\ C & D \end{bmatrix}. \quad (5)$$

From the equations above, \mathbf{C} can be computed by matrix multiplication, and the resulting elements of \mathbf{C} can be used to derive a recursive solution for each 2×2 operation for x (or similarly y) as

$$\begin{aligned} x_{n+2} - 2bx_{n+1} + \gamma x_n &= 0, \\ b &= 1/2(A + D), \quad \gamma = AD - BC = 1. \end{aligned} \quad (6)$$

It can also be shown that $b = \cos(2\theta)$, where 2θ is twice the advance angle defined in Eqs. (1), since this formulation is describing a round trip instead of one pass. The stability criterion for θ to be real also creates the restriction $|b| \leq 1$, from which the allowed confocal separation distance is established. The angle θ is the centroid of revolution of the x or y component. For the astigmatic Herriott cell (without rotation), there are separate solutions for θ_x and θ_y , so that reentrant solutions must satisfy two simultaneous equations.

If the principal axis of a nonspherical mirror is not aligned with x or y , but twisted by an angle δ , then a 4×4 matrix must be used to include cross terms (coupling of x and y), and the rotation matrix for this situation is defined by $\mathbf{R}' = \mathbf{T}(-\delta) \cdot \mathbf{R} \cdot \mathbf{T}(\delta)$, where¹²

$$\mathbf{T}(\delta) = \begin{bmatrix} \cos \delta & 0 & \sin \delta & 0 \\ 0 & \cos \delta & 0 & \sin \delta \\ -\sin \delta & 0 & \cos \delta & 0 \\ 0 & -\sin \delta & 0 & \cos \delta \end{bmatrix}. \quad (7)$$

This rotated reflection matrix and the 4×4 translation matrix must be used when either mirror is rotated away from an orthogonal axis. Note that this generalized matrix approach can be used for any two-mirror system.

From the formulations presented above, generalized analytic solutions similar to Eq. (6) can be derived for rotated mirror systems, where the position of each spot for the n th round trip is given by a recursion formula. Unfortunately, these are very complicated algebraic expressions and the matrix formulation for these systems is preferred.

D. Cylindrical-Cylindrical Mirror System

Turning now to the cylindrical mirror pair (Fig. 1), let us define the starting point for this system with the

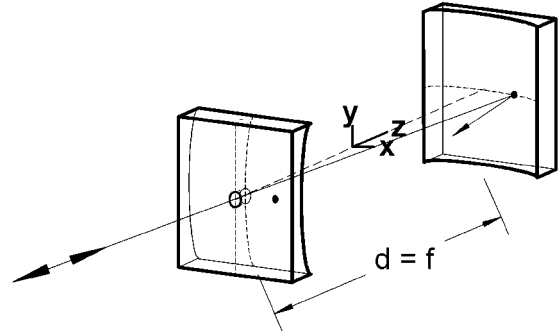


Fig. 1. Cylindrical-cylindrical mirror cell having an on-axis input hole, set for an initial alignment condition of four passes, with focal lengths initially orthogonal.

two mirrors twisted at a relative angle of $\delta = 90 \text{ deg}(\pi/2)$, so that the front mirror has curvature along the y axis and the rear mirror is curved along the x axis. This matched orthogonal cylindrical cell behaves in a manner similar to the spherical Herriott cell as follows.

Since the curvatures of the two mirrors are orthogonal and independent, this $\pi/2$ crossed cylindrical system can be represented by 2×2 matrices, Eqs. (4) and (5), where the x component for \mathbf{R}_1 uses 0 and \mathbf{R}_2 uses $1/f_1$ for the inverse focal lengths, and along the y component \mathbf{R}_1 uses $1/f_2$ and \mathbf{R}_2 uses 0. We note that if the cylinders were aligned, the beams would always walk off the edge along the flat mirror dimension. For the special case using cylindrical mirrors of equal focal lengths and solving for b and γ in Eq. (6), the formulas for reentrant θ and the stability criteria as discussed earlier become

$$\theta_R = \cos^{-1}(\sqrt{1 - d/2f}), \quad 0 \leq d \leq 2f. \quad (8)$$

Valid solutions can be characterized as $N = 8M + K$ for this special system, where θ_R is equal to $\pi M/N$ for a central input hole (linear patterns of spots) and $2\pi M/N$ for off-axis entry (elliptical patterns of spots). As with the normal spherical mirror cell, additional restrictions on allowed values of K exist to avoid common factors upon reentry. The additional restriction for a center (on-axis) hole is that $N/2$ must be odd. For the case of unequal focal lengths aligned orthogonally, the dense Lissajous patterns of Hao are observed, although these will not be reentrant unless stringent specifications for the focal lengths are met.

To our knowledge, in all prior uses of spherical and astigmatic Herriott cells, the laser was injected through the input mirrors with normalized slopes $x_0' = \pm 1, y_0' = \pm 1$ for on-axis systems [$x_0 = 0, y_0 = 0$] and $x_0' = \pm 1, y_0' = -1$ for off-axis cells [$x_0 = 0, y_0 = 1$]. However, for cylindrical mirror cells, we find more a useful input slope condition to be $x_0' = \pm 1, y_0' = 0$ for both on- and off-axis systems, relative to the input configurations presented. These create the widest dispersion and greatest symmetry of spot patterns. Figure 2 shows the relative reen-

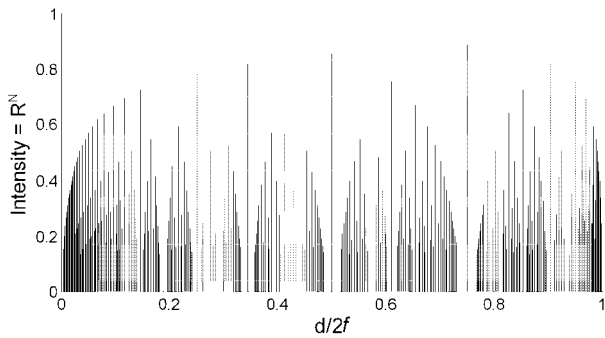


Fig. 2. Plot of relative reentrant intensity for a cylindrical-cylindrical mirror cell as a function of dimensionless mirror separation $d/2f$, with the mirror axes at $\delta = \pi/2$ and an off-axis input hole.

trant laser intensity as a function of reduced mirror separation $d/2f$ for a cylindrical mirror cell at 90 deg with an off-axis hole. The relative intensity of the light exiting the cell is related to N by R^N , where $R = 0.98$ is the mirror reflectivity in this calculation. As compared with conventional Herriott cells, these patterns of N versus $d/2f$ are similar but not identical.

When one of the mirrors is now rotated away from $\delta = 90$ deg, dense Lissajous patterns appear, both for equal and unequal focal length mirrors. Here the 4×4 matrix or the more detailed analytic solutions are required in order to compute spot patterns and predict reentrant conditions, as the x and y solutions are now coupled. Nevertheless, the analysis is somewhat simpler than for the astigmatic system. In particular, for two cylindrical mirrors of equal focal lengths with a centered input hole, it is convenient to describe the reentrant angles as a function of the input parameters

$$\cos(2\theta_{xR}) = \frac{1}{2}(F - \xi), \quad \cos(2\theta_{yR}) = \frac{1}{2}(G + \xi), \quad (9)$$

where

$$F = 2\left(\frac{d}{f} \cos^2\tau - 1\right)^2 - \left(\frac{d}{f}\right)^2 \cos^2\tau,$$

$$G = 2\left(\frac{d}{f} \sin^2\tau - 1\right)^2 - \left(\frac{d}{f}\right)^2 \sin^2\tau,$$

$$\xi = \frac{1}{2}(G - F) \left\{ -1 + \left[1 - \frac{4\varepsilon^2}{(G - F)^2} \right]^{1/2} \right\},$$

$$\varepsilon = -\left(\frac{d}{2f}\right)^2 \sin(4\tau), \quad \tau = \frac{\delta}{2}.$$

Given a set of mirrors with focal lengths f and a desired set of advance angles $\theta_x = \pi M_x/N$, $\theta_y = \pi M_y/N$, one can solve Eqs. (9) to determine the necessary mirror separation d and twist angle δ needed to achieve the desired number of passes. Note

that all solutions depend only on the ratio of d/f , not on the absolute value of the focal length as for astigmatic or the orthogonal mismatched cylindrical cells.

Using reduced coordinates for mirror separation d/f , one can compute plots of spot patterns on each mirror for any values of d and δ . Examination of these patterns in terms of input conditions, exit slopes, overlapping spot patterns, etc. allows us to characterize this matched cylindrical system as follows. In this discussion, we assume that the front mirror will be rotated away from the orthogonal axes, that the curvature on this mirror is initially in the y - z plane, and that the curvature on the rear mirror is fixed in the x - z plane.

1. Center Input Hole Solutions

For a central input hole, all input slopes that keep the pattern on the mirrors are useful. However, we find that the optimal input slope for a cylindrical mirror pair is one where the first pass spot position in normalized units is $x_1 \approx \pm 1$ and $y_1 \approx 0$ (i.e., $[x'_0 \approx \pm 1, y'_0 = 0]$). In practice this means that the input beam points in the horizontal plane to near the edge of the rear mirror at a separation distance d equal to f . Under these conditions, the mirror areas are most efficiently filled to allow the greatest separation of spots. The patterns are square and symmetric.

There are reentrant solutions for all integer values of M_x and M_y . N is even, since here we consider only solutions with one mirror hole. However, not all allowed solutions are equally useful, and there are three categories for M_x, M_y pairs.

First, the most useful case is where both M_x and M_y are even integers. The beam always exits as the mirror image of the input beam relative to the input plane, as is the case for a standard Herriott cell. For example, if the input beam position some distance behind the front input mirror hole is at coordinates $[x_{in}, y_{in}]$, then the output beam at the same distance from the mirror will be found at $[-x_{in}, -y_{in}]$. Also, the output spot is essentially invariant to minor misadjustments to the mirror tilt alignment for this case, similar to the behavior for spherical Herriott cells with this reentrant behavior (equal coefficients along the diagonal of the transfer matrix $C_{N/2}$). Within this case, we also find that the $(N/2)$ th spot always lies at the mirror center $[x_{N/2} = 0, y_{N/2} = 0]$. For $N/2$ even, the $(N/2)$ th spot lies centered on the front mirror and exits early on this pass, rather than on the N th pass; thus these patterns of N are not allowed. However, for $N/2$ odd, this $(N/2)$ th spot will always be found at the rear mirror center position. This is very useful for recognizing when a valid reentrant pattern is achieved.

Second, if M_x and M_y are both odd numbers, then the reentrant output beam always exits back exactly along the input beam path and travels back to the light source. While not useful for absorption measurements, this may be very useful for applications in which a long optical feedback path returning to the laser source is desired.

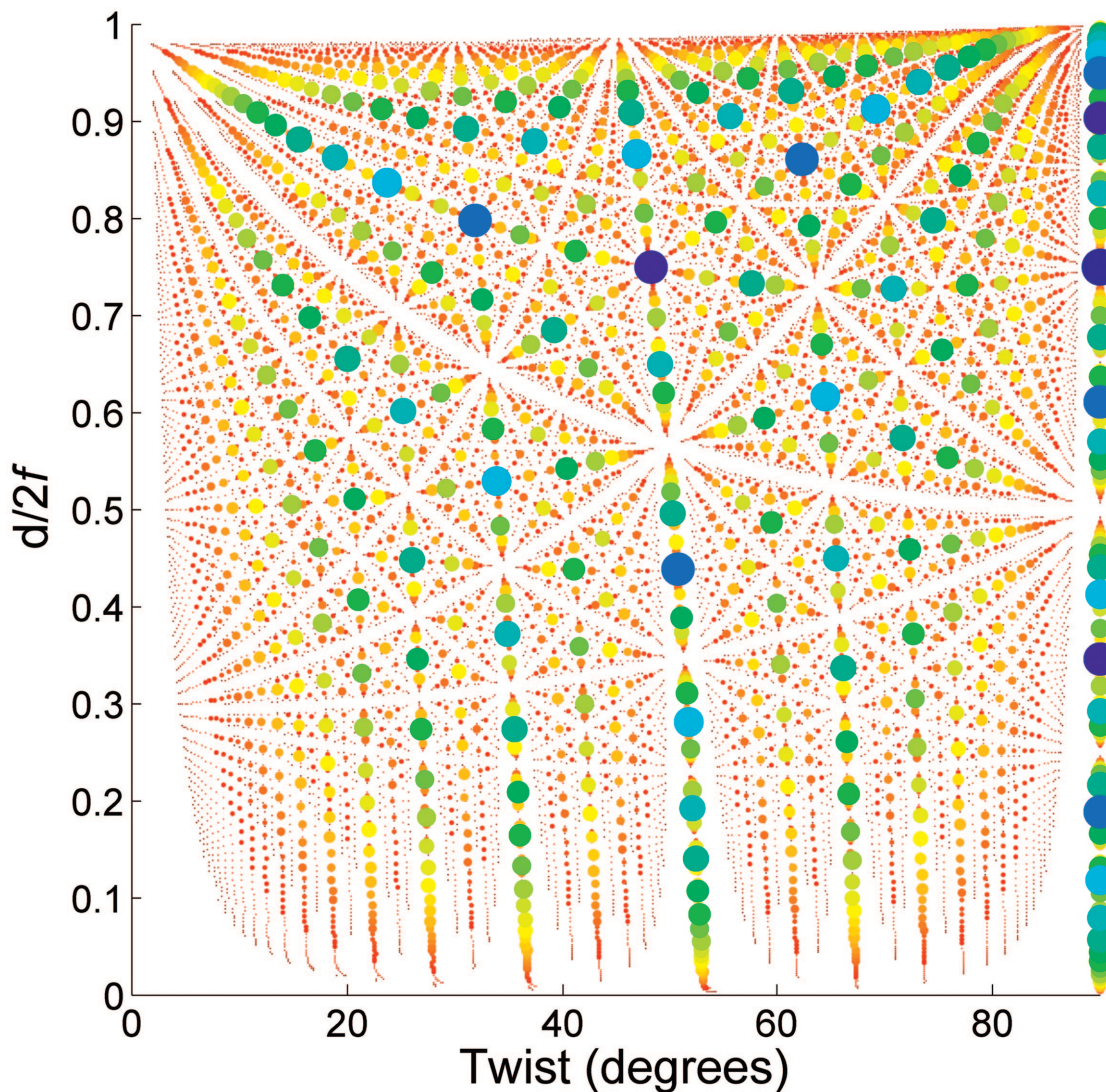


Fig. 3. Map of allowed reentrant pass number as a function of mirror separation d and mirror twist angle δ . The magnitude of N is denoted (logarithmically) by the diameter of each spot and by color ranging from dark blue (6 passes, largest) to red (200 passes, smallest).

The final case occurs when M_x is even and M_y is odd, or vice versa. The output beam exits the cell at coordinates that vary in the x - y plane, depending on the values of M_x , M_y , and N . Since there is no simple *a priori* prediction of where these positions lie, this is less useful than the first case for applications that would typically benefit from a Herriott-style cell.

A further restriction on allowed spot patterns is degeneracy of higher-order patterns that are multiples of lower-order patterns. In the general case for N passes, when any $N_{\text{even}}' < N$ exists such that for both x and y , $[N_{\text{even}}' \theta_{x,y}]_{\text{mod } \pi} = 0$, then that $\{N, M_x, M_y\}$ configuration is not allowed. This is equivalent to the restrictions found for other Herriott systems.^{2,11,12}

Figure 3 is a map of allowed reentrant solutions for up to 200 passes for a cylindrical mirror cell having a center input hole. Since this system is symmetric in twist angle about $\pi/2$, only the first quadrant of twist is shown. The relative sizes of the symbols inversely scale logarithmically as the number of passes N ,

where N varies from 6 (largest symbol) to 200 (smallest). Clearly, there are many possible solutions for any desired number of passes, independent of the precise value of the focal length.

2. Off-axis (Edge) Input Hole Solutions

For an edge input hole, reasonable initial slopes are those that cause the spot pattern to be confined to the mirror surfaces. So for $[x_0 = 0, y_0 = 1]$, the initial beam slopes are generally defined so that the spot position after the first pass has $-1 < x_1 < 1$ and $0 < y_1 < r$, where r is the radius of the mirror. However, for an input beam with $[x' = \pm 1, y' = 0]$ the spot pattern is optimally spaced and diamondlike for twist angles other than 90 deg. At 90 deg, patterns are optimally circular at $d = f$ and follow elliptical paths at other mirror separations, similar to the spherical mirror Herriott patterns.

Only even pairs of M_x, M_y with $N/2 = \text{odd}$ give reentrant solutions for off-axis systems. For odd-odd,

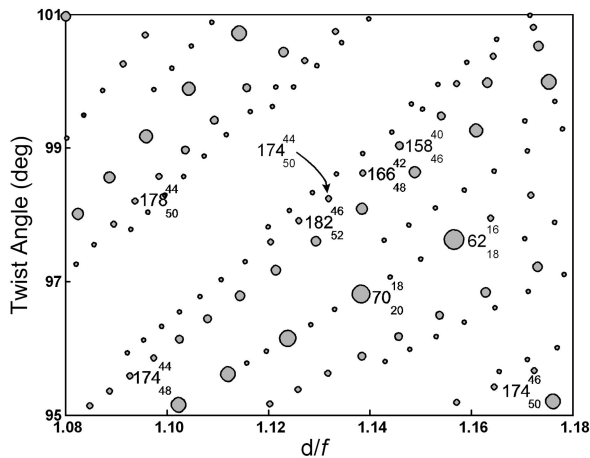


Fig. 4. Map of allowed reentrant pass number as a function of separation $d/f =$ near 1.1 and mirror twist angle δ near 98 deg. Selected spots are denoted by the indices $N_{M_x}^{M_y}$.

even-odd, or odd-even pairs, the N th spot hits the front mirror at some multiple of 90 deg away from the input hole, and these solutions are not allowed. As with all other Herriott-style cells, additional restrictions on M values occur due to lower-order degeneracies. Off-axis entry for dense patterns are in general not as useful as for on-axis cells, since here there are often spots very close to the input hole that either could be clipped and create interference fringes or just exit early.

3. Understanding Relationships Between M Indices and Spot Patterns

To identify spot patterns from observed systems by using the computed patterns, it helps to better understand how the variables (M_x , M_y , N , d , and δ) are interrelated. Focusing on the $N/2$ odd system for now (although similar rules apply to all systems), we find that for a stable cavity $0 < d < 2f$, $M_x + M_y \leq N$. Since the mirror rotations are symmetric about a twist angle of $\pi/2$, so are spot patterns. From a mathematical standpoint, as the mirror system is defined, $M_x > M_y$ corresponds to $\delta < \pi/2$, $M_x < M_y$ to $\delta > \pi/2$, and $M_x = M_y$ to the degenerate system at $\delta = \pi/2$. In general, for any specified N , lower values of M_x and M_y correspond to smaller values of d . Solutions where $d \sim f$ have indices whose sum is near $N/2$. The difference $M_x - M_y$ is a measure of the twist angle—large differences correspond to solutions near $\delta = 0$ or π , and smaller differences have solutions lying near $\delta = \pi/2$. Figure 4 is an enlargement of Fig. 3 near $\delta = 98$ deg and $d/f = 1.1$. If we decide to configure our system for 174 passes and want the mirror separation and twist angle to lie in the region shown in this figure, then these rules help in estimating the values of M_x and M_y required, so that the observed pattern can be confirmed readily by computation.

4. Range of Allowed Solutions

Following the suggestion of McManus *et al.*,¹² the advance angles can be expressed relative to $\pi/2$,

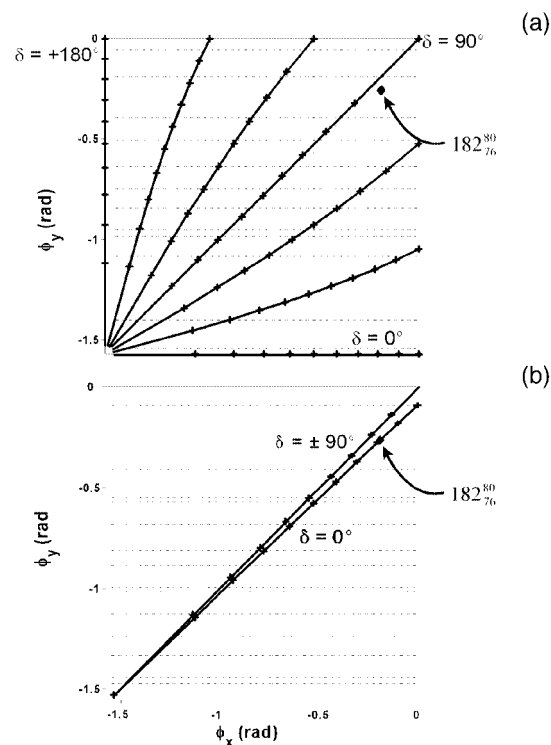


Fig. 5. Plot of reentrant solutions for 182 passes as a function of reduced advance angles ϕ_x and ϕ_y for (a) matched cylindrical cell and (b) astigmatic cell. Solutions for various twist angles shown as solid lines and curves.

$$\phi_{x,y} = \theta_{xR,yR} - \frac{\pi}{2} = \pi \left(\frac{M_{x,y}}{N} - \frac{1}{2} \right). \quad (10)$$

One can plot the possible solutions for a given mirror system as a function of ϕ_x and ϕ_y . An example of this is shown in Fig. 5, restricted to solutions only of 182 passes. All combinations of even M_x and even M_y that generate 182 passes are shown as individual spots. Since the ϕ are linearly proportional to M , these spots are evenly spaced on a grid pattern. The specific solution for $N_{M_x}^{M_y} = 182_{76}^{80}$ is denoted by the solid diamond. This plot is independent of the type of dense mirror system.

If one restricts the solutions to allowed confocal mirror separations, then, using Eqs. (9) and (10) for the cylindrical mirror cell, we find that virtually any solution for N passes can be found over the full range of twist angles δ and separations d . The solid lines in Fig. 5(a) denote the twist angle in increments of 30 deg at which any particular solution is found, and the tick marks on each line correspond to the mirror separation in increments of $0.1 \times 2f$. In the example illustrated for $N_{M_x}^{M_y} = 182_{76}^{80}$, this solution is achieved when $d = 1.90f$ and $\delta = 85.9$ deg.

For comparison, the astigmatic cell (using McManus' design¹²) is shown in Fig. 5(b). In this case the range of allowed solutions is not the entire ϕ_x , ϕ_y space but is greatly restricted to a narrow wedge. Since allowed solutions lie only between these two lines, many fewer possible solutions exist for the 182

pass system shown than for the cylindrical system. In generalizing this to all other N -pass systems, especially lower values of N where the dots (solutions) are more widely spaced and are less likely to lie within the bounded area, the astigmatic cell exhibits less ability to achieve a wide range of viable paths.

The reason for this behavior is the relative focal power along the orthogonal axes of the mirrors. For an astigmatic cell, the x and y components are typically 10% different in focal length, and twisting one of the mirrors has only a mild effect on mixing these components—hence the weak dependence on twist angle. By contrast, the cylindrical mirrors have a much larger difference in their x - and y -component focal lengths, finite (typically tens of centimeters) and infinite. This supposition is verified by numerical simulations of the astigmatic cell whereby the narrow wedge of allowable solutions in Fig. 5(b) widens as the ratio of f_x to f_y deviates further from near unity.

E. Cylindrical–Spherical Mirror System

Cylindrical–spherical cells have few or no useful allowed reentrant solutions. However, they can still be used to create long optical paths by using near reentrant configurations. To investigate the analytic properties of this system, the cylindrical–spherical mirror cell is defined as having one cylindrical mirror with its curved axis focal length f_{cyl} in the y - z plane and one spherical mirror of focal length f_{sph} . In this case, the input hole is located in the center of the cylindrical mirror, although the spherical mirror could be used for input instead.

This optical system can be simply represented by 2×2 matrices derived from Eq. (5), where the x component of \mathbf{R}_1 uses 0 and \mathbf{R}_2 uses $1/f_{\text{sph}}$ for the inverse focal lengths, and the y component for \mathbf{R}_1 uses $1/f_{\text{cyl}}$ and \mathbf{R}_2 uses $1/f_{\text{sph}}$. Solving for b and γ in Eq. (6), the stability criteria as discussed earlier are

$$0 \leq \left(\frac{d}{2f_{\text{sph}}} \right) \leq 1, \quad x \text{ axis},$$

$$0 \leq \left(1 - \frac{d}{2f_{\text{sph}}} \right) \left(1 - \frac{d}{2f_{\text{cyl}}} \right) \leq 1, \quad y \text{ axis}, \quad (11)$$

where the smaller of the distances for x or y is limiting. Similar to Eq. (6), the spot locations for the n th round-trip are expressed by a recursion formula:

$$x_{n+2} - 2 \left(1 - \frac{d}{f_{\text{sph}}} \right) x_{n+1} + x_n = 0,$$

$$y_{n+2} - 2 \left(1 - \frac{d}{f_{\text{sph}}} - \frac{d}{f_{\text{cyl}}} + \frac{d^2}{f_{\text{sph}} f_{\text{cyl}}} \right) y_{n+1} + y_n = 0. \quad (12)$$

For any specified set of mirrors, we can use the matrix or analytic equations to follow the spot positions on the input mirror for each pass (given the input slope and input hole diameter). If one examines the location of any given spot with pass number N on

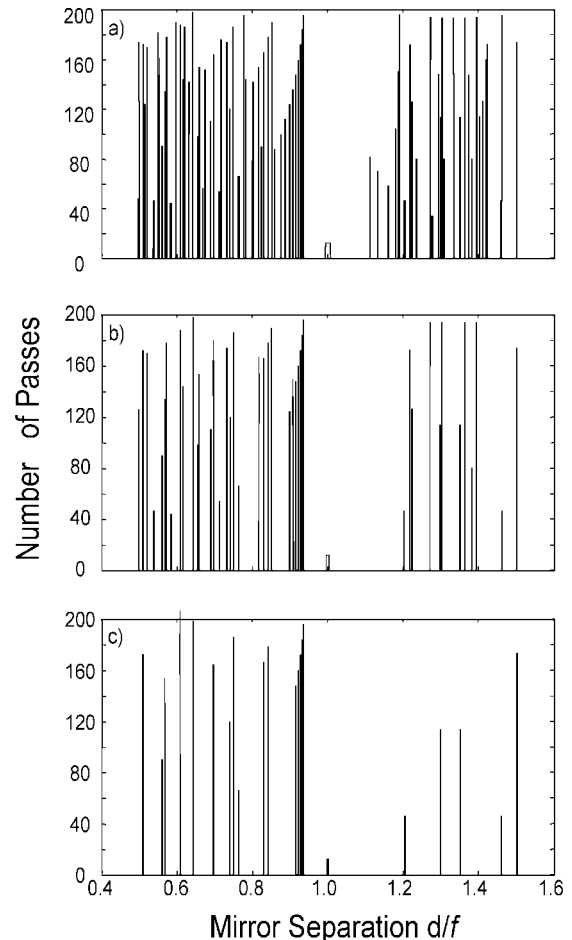


Fig. 6. Plot of exit pass number of a cylindrical–spherical mirror cell as a function of mirror separation $0.5 \leq d/f \leq 1.5$, with the ratio of input hole diameter to maximum spot pattern size being (a) 0.05, (b) 0.025, (c) 0.0125. For this calculation, the same focal length is assumed for both mirrors.

the input mirror as the mirror separation is smoothly varied, its position maps out a Lissajous pattern that at some point crosses the exit hole. After some additional small distance change, it again resumes its trajectory on the mirror surface until its next encounter with the hole. Note that these exit conditions are not necessarily reentrant, they just correspond to ranges of d where the beam exits the cell. The useful (near reentrant) solutions are those where the exiting beam nearly crosses the center of the output hole so that the beam is not clipped. In contrast to prior expectations for Herriott cells, these near reentrant solutions can be easily predicted and found.

Figure 6 is a plot of the near reentrant pass number for beams exiting the cell as a function of mirror separation d and entrance hole diameter, limited to a maximum of 200 passes. In these calculations, the mirror separation is varied from $0.5 < d/f < 1.5$, in steps of $0.008 d/f$, where the focal lengths of both mirrors are kept equal for convenience.

For a large input hole, the beam tends to exit after fewer passes than when the hole is small, since its trajectory is more likely to encounter the bigger hole.

A larger input slope causes the overall spot pattern to cover a larger area, spreading out the spots. Thus the proper scaling factor is the ratio of the hole size to the overall input slope. In addition, since the input slopes are generally maximized to make the pattern as large as possible to best fill the mirrors, then the ratio of the input hole diameter to mirror diameter is also a useful scaling parameter. The variation of near reentrant pass numbers with mirror separation for a few different ratios of the input diameter to the maximum pattern size is shown in Fig. 6. As the hole becomes smaller, trajectories tend toward more passes before exiting the cell, so that fewer solutions below the 200-pass limit are observed.

The exit slope is also important. Like fully reentrant systems, one would like the exiting beam to be physically separated from the input beam so as to permit placement of additional optical components or a photodetector without clipping or blocking the input beam. Figure 7 is a plot of the beam exit locations [using the case of Fig. 6(b)] in the x - y plane just outside the input mirror, computed by noting the exit pass number. Over the small region of d where a given N th spot exits, the spot position moves across the hole as described above, where the circular symbols on each line correspond to individual d/f steps of 0.008. Note that for lower N the spot trajectory travels more slowly across the hole, and for higher N the symbols are more widely spaced as the velocity of the trajectory increases. The input beam location is noted by the \times in quadrant a . The most useful exit conditions are those in which the beams are in the quadrant opposite the input beam, although adjacent quadrants could be used for placing the detector. In any case, any of quadrants b, c, or d has a reasonable number of solutions to be useful for selecting a wide range of N for measurement.

3. Experiment

A pair of 5 cm square cylindrical mirrors with $f = 64.8$ mm (Newport Corporation) was assembled on mounts on an optical rail so that the separation could be smoothly varied. The front mirror was mounted on a rotation stage. As illustrated in Fig. 1, the front mirror is aligned so that the radius of curvature is in the y - z plane, and the rear mirror initially is set with its radius of curvature in the x - z plane. The output of a JDS Uniphase He-Ne visible laser (632.8 nm) was injected through a 4.7 mm diameter hole in the center [$x_0 = y_0 = 0$] of the front mirror such that at $d = f$ the first spot strikes the rear mirror at $x_1 = 25$ mm, $y_1 = 0$ mm (with a slope arbitrarily defined in reduced units as $x_0' = 1, y_0' = 0$). The reflectivity of these mirrors at 632 nm is approximately 0.975. The intensity of the output beam from the cell is monitored by a silicon photodiode. We also performed some measurements in which the rear mirror had a different focal length of 51.9 mm. For real applications of this approach, a smaller-diameter input hole (2.5–3 mm diameter) is probably more appropriate. For the second configuration of a cylindrical-spherical mirror pair, the rear mirror was replaced

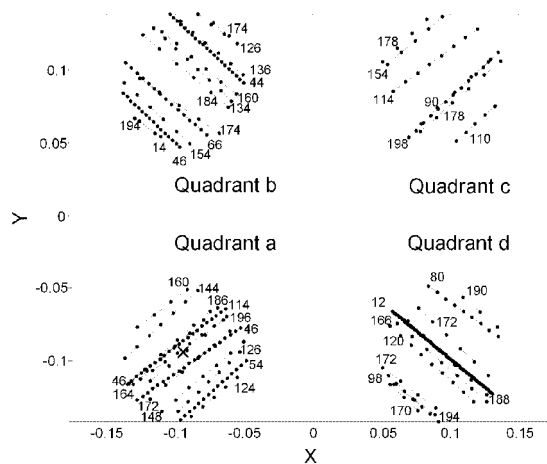


Fig. 7. Plot of beam exit locations in the x - y plane just outside the input mirror for case (b) of Fig. 6, noting the exit pass number and quadrant. The \times in the lower left quadrant denotes the location of the input beam in this plane.

by a 2 in. diameter spherical mirror with $f_{\text{sph}} = 100$ mm.

The distribution of laser beam intensity at various positions in the optical path, particularly after exiting the multiple pass cell, were monitored with a video camera. The images from this camera were displayed on a laptop computer by using Mesa Photonics VideoFrog software.

Wavelength modulation absorption spectra (WMS) of the PQ 9,8 line ($13,093.65 \text{ cm}^{-1}$) of molecular oxygen in room air were taken by using a vertical cavity laser (Avalon Photonics) with the matched cylindrical cell.

4. Results and Discussion

Using the mirror systems as described above, various high-density pass patterns were configured for both a cylindrical-cylindrical mirror pair (both matched and unequal focal length pairs) and a cylindrical-spherical mirror pair (unmatched focal lengths).

A. Cylindrical-Cylindrical Mirror Cell

For the matched cylindrical-cylindrical system, achieving a desired number of passes by first computing patterns (given N , M_x , and M_y) and then setting d and δ was demonstrated, as was configuring patterns by randomly adjusting the mirrors to a dense pattern (setting d and δ) and then determining the number of passes by computing N , M_x , and M_y from the given values.

Here the mirrors are initially set with orthogonal axes at approximately $d = f$ (Fig. 1). The first spot points to [$x_1 \sim 0.8r, y_1 = 0$]. This causes the second pass to travel parallel along the z axis and strike the front mirror at [$x_2 = x_1, y_2 = y_1$]. Since this mirror is flat in the x - z plane (at $y = 0$), the third pass reflects directly back onto spot 1 on the rear mirror and retraces the input beam out of the cell. This alignment can be verified by observing the exit spot superimposed on the input beam on any of the mirrors that

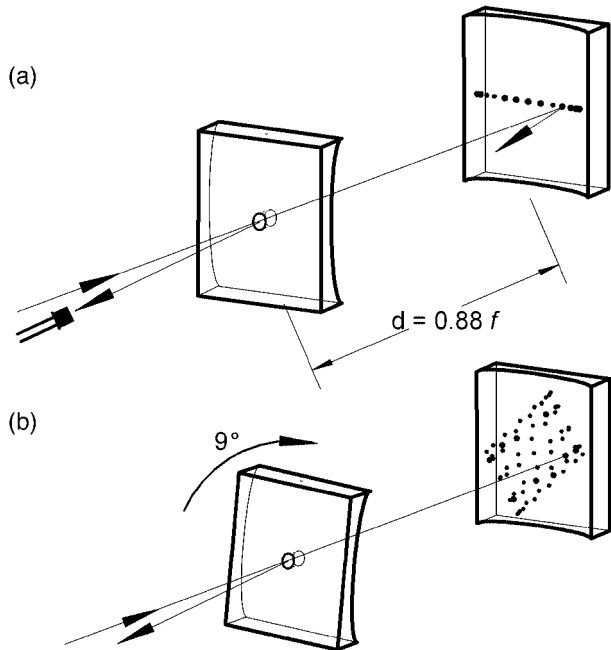


Fig. 8. (a) Spot pattern for 26 passes with a 90 deg crossed cylindrical-cylindrical mirror cell at $d/f = 0.88$. (b) Dense spot pattern of 122 passes created by rotating front mirror by 9 deg.

point the incoming beam into the cell. In terms of cell indices, this condition is characterized by $N_{M_x}^{M_x} = 4_1^1$. As the mirror separation is moved away from $d = f$, all spot patterns should be observed as horizontal lines. If any patterns appear two dimensional, then a minor twist angle rotation of the front mirror or tilting of one of the mirrors can be used to quickly flatten the pattern to the desired linear shape. Once accomplished, the mirrors are then exactly parallel, orthogonal, and properly aligned.

If one were using an off-axis entry hole position (such as $x_0 = 0, y_0 = 1$), then there would be an eight-pass reentrant condition ($N = 8, K = 0, M = 1$) with a rectangular pattern on the back mirror and a diamond on the front. Note that this assumes the same beam entry slope as with the center hole scheme. Other input slopes would give different patterns, but all could be calculated and used for initial alignments.

Now using the center-hole input, as the mirror separation is moved away from $d = f$, a series of horizontal spot patterns are observed, corresponding to a flattened normal Herriott pattern. Since these spots are easily counted, we can use these as a guide (as well as measure mirror separation) to determine where we are in d - δ space before rotating the twist angle to achieve dense spot patterns. We also note that the allowed output spot patterns ($N/2$ odd) have a constant output beam position, and we can align the detector now using the output beam for any $N/2$ odd pattern.

Figure 8(a) shows an unrotated ($\delta = \pi/2$) spot pattern of $N = 26$ with $d/f = 0.88$, where the beam exits the cell and strikes the photodiode at a fixed

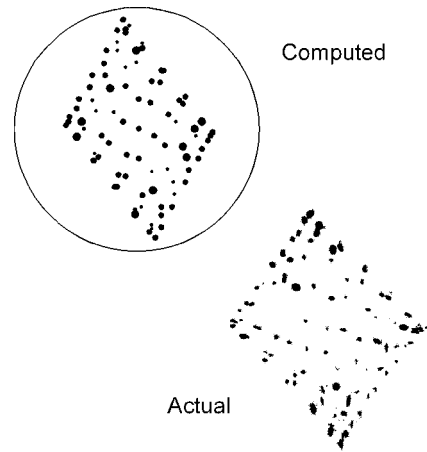


Fig. 9. Plot of a 174-pass dense spot pattern computed and observed at $d/f = 1.13$ and mirror twist angle $\delta = 98.3$ deg.

position. A rotation of the front mirror by ~ 9 deg leads to a dense 122-pass spot pattern [Fig. 8(b)].

One aid in identifying allowed patterns is that they all exhibit a centrally located spot [$x_{N/2} = y_{N/2} = 0$] on the rear mirror, always corresponding to the $(N/2)$ th pass. As with other Herriott-type cells, this particular configuration is insensitive to mirror tilt. Many similar patterns can be achieved by various combinations of separation and rotation as predicted from the calculations illustrated in Fig. 3.

For example, if we look at an enlarged portion of this map near $d = 1.1 \times f$ and $\delta = 98$ deg (Fig. 4), we see a variety of solutions and that the $N_{M_x}^{M_x} = 174_{50}^{44}$ system should be positioned at $d/f = 1.132$ and $\delta = 98.25$ deg. From the formulas (either matrix or analytic) we can compute the expected spot pattern shown in Fig. 9. After adjusting the mirror system to these d/f - δ conditions, the desired pattern matching this computation is achieved, as shown by the photograph (Actual) in this figure. Conversely, one can also just set the mirrors to some desired pattern and then computationally identify $N, M_x,$ and M_y . Measurements involving a cylindrical cell with mismatched focal lengths produced similar results, where patterns could be computed by using the matrix formulations and then set up in the lab.

The increased symmetry of the cylindrical cell permits the possibility of much easier alignment and assignment of patterns and certainly more flexibility in choosing patterns for a given system. This is particularly true for a matched pair of cylindrical mirrors. The cylindrical cell permits virtually any solution for a given mirror pair, since the solutions depend on the ratio of d to f , not on the absolute values of focal lengths. Whenever $M_x = M_y$, the system is degenerate, and all solutions are those of the 90 deg crossed cylindrical mirror system.

A $2f$ WMS absorption spectrum of the PQ 9,8 line of O_2 is shown in Fig. 10. This corresponds to a total path of 7.06 m (including 71 cm of external path) and 142 passes of the dense cell. This pattern was found by starting with a 10-pass linear configuration (d/f

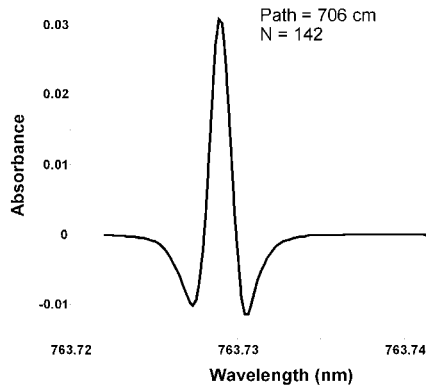


Fig. 10. $2f$ WMS absorption spectrum of O_2 near 763 nm in cylindrical multipass cell with $N = 142$.

= 0.69) with subsequent rotation of the mirror by 17.3 deg. Although the VCSEL output beam is visible, its low power made direct visualization of the mirror spots difficult (as would any infrared laser as well), so a coaligned He–Ne laser was used in initial alignment. Using a flip-down mirror, the He–Ne laser traced the same path as the VCSEL from the mirror, pointing the beam into the cell and to the first pass spot position on the rear mirror. Using a 10-pass or 26-pass configuration to get the He–Ne onto the detector, the VCSEL laser beam was now also aligned. Using an infrared sensor card (Newport), one could verify that the VCSEL had the same spot positions as the He–Ne. From this point on, dense patterns could be readily found by adjusting the mirror separation and rotation angle.

While no evidence of etalons (interference fringes) in these spectra were observed, these cells could be a source of interference fringes. The same caveats that apply to other multiple-pass cells also apply here. Selection of spot patterns that place all spots further from the entrance hole are preferred, and making the entrance beam waist diameter reasonably smaller than the hole size should minimize scattering and backreflections.

Since one might expect distorted output beam shapes with cylindrical mirrors, a random set of $N/2$ odd, M_x even, M_y even output beam intensity distributions were measured by using the video camera. These spots were found to be essentially round in all cases, and as might be expected for these reentrant conditions, were located at the same spatial position.

B. Cylindrical–Spherical Mirror Cell

For the cylindrical–spherical mirror pair, the goal is to create near reentrant patterns with this simpler system. The initial setup is similar to the cylindrical mirror pair. We point the input beam to a position $[x_1 \sim r/2, y_1 = 0]$, i.e., a nominal slopes of $[x_0' = 1, y_0' = 0]$. Since the source of the first spot on the spherical mirror originates at a distance equal to its focal length, the reflected beam is then collimated (parallel) to the cell's z axis and strikes the input mirror coordinates $[x_2 = x_1, y_2 = y_1 = 0]$. The cylin-

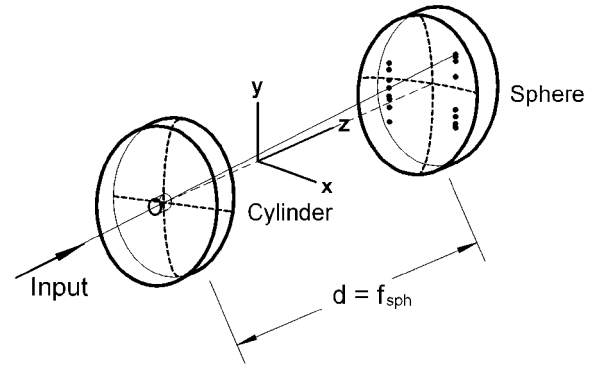


Fig. 11. Cylindrical–spherical mirror cell having an on-axis input hole and set for an initial alignment condition having two rows of spots.

dricul mirror is flat along the x axis at $y = 0$ and, as before, acts as a flat mirror, causing the beam to retrace its initial path back to spot 1 (pass number 3) and out through the center of the input hole (pass four) exactly aligned along the path of the input beam. This four-pass (fully reentrant) alignment condition is very simple and permits the initial proper settings of tilt adjustments and separation of the mirrors to make them parallel and define the separation axis.

If the input slopes are now adjusted to $[x_0' \approx 0.7, y_0' \approx 0.7]$, a spot pattern appears as illustrated in Fig. 11. We note that although this mirror system is insensitive to rotation of one mirror relative to the other (unlike any of the other dense pattern multiple-pass cell methods), rotation of the entire cell (or equivalently, rotation of the cylindrical mirror only, since the spherical mirror is fully symmetric about the rotation axis) is identical to changing the input slopes as long as the radial distance from the center of the rear mirror to spot 1 is unchanged. As a result, this new set of slopes results in patterns fully equivalent to those observed if instead the cylindrical mirror axis had been rotated by 45 deg relative to the initial input slopes. In this case, a near reentrant dense pattern comprising two lines of spots is observed on the rear mirror, for a total of 36 passes before exiting the cell.

Other dense patterns of spots can be found by varying the mirror separation. For example, Fig. 12 compares a photo (Actual) with computed pattern for $N = 166$ passes when the separation $d = 98.1$ mm. In this case the output beam still passes within 0.5 mm of the hole center. At a distance 5 cm behind the hole, the separation of input and output beams is ~ 2 cm, certainly well enough separated to locate a photodiode detector or collection optic. With other mirror separations and input slopes, many different useful near reentrant patterns can be readily found.

None of the input hole diameter, slope, or mirror separations are restricted, except by stability constraints and by physical dimensions to be sure that all spots hit a mirrored surface. However, the better choices are to keep d approximately between 0.5 and

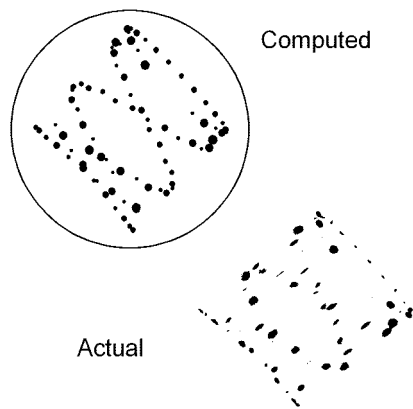


Fig. 12. Cylindrical-spherical mirror cell dense spot pattern computed and observed for 166 passes.

1.5 times the mean focal length and the input hole diameter below 10% of the mirror diameters.

C. Other Useful Multipass Configurations

As a final comment regarding the use of Herriott-style multiple-pass cells, a few other variations have proved useful in some of our instruments. First, one can use a flat-mirror-spherical-mirror pair to replace a conventional spherical pair Herriott cell. In essence, this is equivalent to placing a flat mirror in the center of the conventional cell, causing the rear spot pattern to be reflected and superimposed on the front mirror pattern. In this case, allowed solutions are identical to those for the off-axis fully cylindrical cell given in Eq. (8), with lower-order restrictions on $\{N, M, K\}$ similar to those for a normal Herriott cell. In this case a better set of entry slope conditions to use involves setting $y' = 0$ so that the first pass is parallel to the $x-z$ plane, assuming that the hole is located in the top center region of the mirror [$x_0 = 0, y_0 = 1$]. This different slope makes alignment much easier and permits one to get nearly circular patterns for a variety of families of K , rather than tight ellipses.

Another simplification one can make for the off-axis input designs is to use square or rectangular front mirrors (particularly suited to flat or cylindrical mirrors, where these shapes are readily available) as the input to the cell. In this case the input and output beams can be configured to enter just outside of the mirror edge, while all intermediate passes still strike the mirror. The advantage to this design is that no holes need be drilled through any optics.

Finally, we note that in optical systems where one is trying to make a one-dimensional measurement (e.g., measuring concentration profiles across a flat flame burner where concentrations in the $x-z$ plane are uniform but vary with height), a multiple-pass system such as the matched orthogonal cylindrical pair with central input hole will provide a truly linear pattern of spots. Thus one can get the multipass path advantage without sacrificing vertical resolution accuracy.

5. Conclusions

The present cylindrical mirror-based designs provide a simpler, lower-cost, and more easily aligned approach for constructing high-density multipass optical cells, where many different configurations can be achieved with the same set of mirrors. Unlike the astigmatic cell or mismatched orthogonal cylindrical cell, the cylindrical mirror pair system does not rely on the absolute manufactured focal lengths, but only on the easily adjusted ratio d/f and relative twist angle of the two cylindrical axis planes. For the cylindrical-spherical mirror pair, it is shown that even near reentrant solutions are viable for multipass cells. These designs should be useful for optical absorption, Raman gain, photoacoustic, and laser feedback applications.

This work was performed under Department of Energy Contract DE-FG02-03ER83779 and NASA Contract NNA04CB22C. The author also thanks David Bomse and Chris Hovde for helpful discussions.

References

1. J. U. White, "Long optical paths of large aperture," *J. Opt. Soc. Am.* **32**, 285–288 (1942).
2. J. Altmann, R. Baumgart, and C. Weitkamp, "Two-mirror multipass absorption cell," *Appl. Opt.* **20**, 995–999 (1981).
3. D. R. Herriott and H. J. Schulte, "Folded optical delay lines," *Appl. Opt.* **4**, 883–889 (1965).
4. W. R. Trutna and R. L. Byer, "Multiple-pass Raman gain cell," *Appl. Opt.* **2**, 301–312 (1980).
5. D. Herriott, H. Kogelnik, and R. Kompfner, "Off-axis paths in spherical mirror interferometers," *Appl. Opt.* **3**, 523–526 (1964).
6. M. W. Sigrist, A. Bohren, I. G. Calasso, M. Nägele, A. Romann, and M. Seiter, "Laser spectroscopic sensing of air pollutants," in *13th Symposium and School on High-Resolution Molecular Spectroscopy*, L. N. Sinita, ed., *Proc. SPIE* **4063**, 17–25 (2000).
7. A. Yariv, "The propagation of rays and spherical waves," in *Introduction to Optical Electronics* (Holt, Reinhart, & Winston, New York, 1971), pp. 18–29.
8. M. M. Salour, "Multipass optical cavities for laser spectroscopy," *Laser Focus* **13**(10), 50–55 (1977).
9. S. M. Chernin and E. G. Barskaya, "Optical multipass matrix systems," *Appl. Opt.* **30**, 51–58 (1991).
10. R. M. Abdullin and A. V. Lebedev, "Use of an integrating sphere as a multiple pass optical cell," *Sov. J. Opt. Technol.* **55**, 139–141 (1988).
11. J. B. McManus and P. L. Kebebian, "Narrow optical interference fringes for certain setup conditions in multipass absorption cells of the Herriott type," *Appl. Opt.* **29**, 898–900 (1990).
12. J. B. McManus, P. L. Kebebian and M. S. Zahniser, "Astigmatic mirror multipass absorption cells for long-path-length spectroscopy," *Appl. Opt.* **34**, 3336–3348 (1995).
13. P. L. Kebebian, "Off-axis cavity absorption cell," U.S. Patent 5,291,265 (1 March 1994).
14. L.-Y. Hao, S. Qiang, G.-R. Wu, L. Qi, D. Feng and Q.-S. Zhu, "Cylindrical mirror multipass Lissajous system for laser photoacoustic spectroscopy," *Rev. Sci. Instrum.* **73**, 2079–2085 (2002).
15. J. A. Silver, "Dense pattern optical multipass cell," U.S. patent application 10/896,608 (21 July 2004) and "Near re-entrant dense pattern optical multipass cell," U.S. patent application 10/948,660 (22 September 2004).